Chemistry Europe
European Chemical Societies Publishing

Mesoporous Silica Nanoparticles Functionalized with Amino Groups for Biomedical Applications

Bianca Martins Estevão,[a, b, c] Ivana Miletto,*[a] Noboru Hioka,[b] Leonardo Marchese,[a] and Enrica Gianotti*[a]

The synthesis and characterization of amino-functionalized mesoporous silica nanoparticles are presented following two different synthetic methods: co-condensation and post-synthesis grafting of 3-aminopropyltriethoxysilane. The amino groups' distribution on the mesoporous silica nanoparticles was evaluated considering the aggregation state of a grafted photosensitizer (Verteporfin) by using spectroscopic techniques. The homogeneous distribution of amino groups within the silica network is a key factor to avoid aggregation during further organic functionalization and to optimize the performance of functionalized silica nanoparticles in biomedical applications. In addition, the formation of a protein corona on the external surface of both bare and amino-functionalized mesoporous silica was also investigated by adsorbing Bovine Serum Albumin (BSA) as a model protein. The adsorption of BSA was found to be favorable, reducing the aggregation phenomena for both bare and amino-modified nanoparticles. Nevertheless, the dispersant effect of BSA was much more evident in the case of amino-modified nanoparticles, which reached monodispersion after adsorption of the protein, thus suggesting that amino-modified nanoparticles can benefit from protein corona formation for preventing severe aggregation in biological media.

1. Introduction

In recent years, great efforts have been devoted to the synthesis and characterization of organic-inorganic hybrid systems. These hybrids are the subject of many studies due to their great versatility and thanks to the variety of organic groups which can be readily attached through chemical bonds, as, for example, in the present case to mesoporous silica nanoparticles. In this way, tuning of the physicochemical properties is possible with the objective of obtaining functionalized materials that can be used as platforms for the binding of molecules with interesting applications in many fields, such as drug delivery, catalysis, sensors and photovoltaics.[1–3] Two main methods for the synthesis of silica-based organic-inorganic hybrids are usually proposed: co-condensation or grafting of the organic moieties (Scheme 1). Co-condensation is the functionalization of the inorganic support by adding the organic group directly in the synthesis gel, that is, a single-stage process called "one-pot", whilst grafting is a post-synthesis treatment, where the organic function is covalently attached to the inorganic network through silanol groups.[4,5] After the surfactant removal by calcination, the desired organic group can be "grafted" using several types of molecules bearing a terminal group which can readily react with surface silanols, such as alkoxysilanes, characterized by the general formula $(RO)_3Si\text{-}R'$, chlorosilanes $Cl_3Si\text{-}R$ or silazanes $HN\text{-}(Si\text{-}R_3)_2$. Chlorosilanes and silazanes are very reactive and moisture-sensitive; thus, self-condensation often occurs during the functionalization process. On the

[a] Dr. B. M. Estevão, Dr. I. Miletto, Prof. Dr. L. Marchese, Prof. Dr. E. Gianotti
Department of Science and Technological Innovation
Università del Piemonte Orientale
Viale T. Michel, 11 – 15121, Alessandria (Italy)
E-mail: ivana.miletto@uniupo.it
enrica.gianotti@uniupo.it
[b] Dr. B. M. Estevão, Prof. Dr. N. Hioka
Research Nucleus in Photodynamic System
State University of Maringá
Av. Colombo, 5790 CEP 87020–900, Maringá, Paraná (Brazil)
[c] Dr. B. M. Estevão
Group of Nanomedicine and Nanotoxicology
São Carlos Institute of Physics, University of São Paulo
Av. Trabalhador São-carlense, 400 CEP 13566–590, São Carlos (Brazil)

Supporting information for this article is available on the WWW under https://doi.org/10.1002/open.202100227

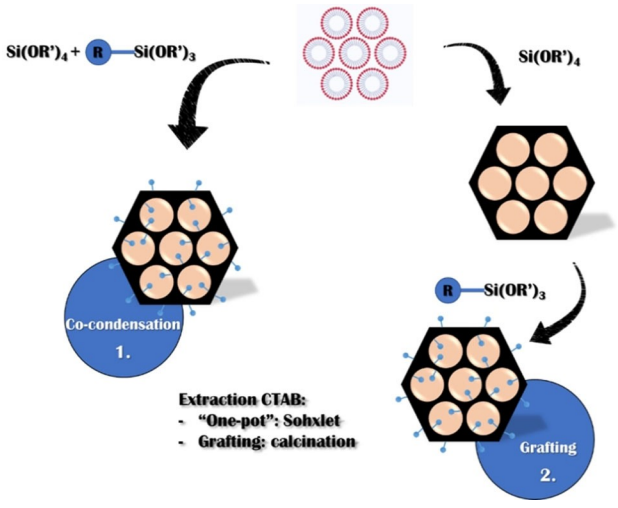

Scheme 1. Preparation of organic-inorganic hybrid mesoporous silica nanoparticles by co-condensation (1) and grafting (2).

contrary, alkoxysilanes are less reactive and thus are easier to control in the functionalization process. Usually, methoxysilanes or ethoxysilanes are used, for which the reactivity decreases with increasing alkyl chain length. According to the concentration and alkyl chain size, the hydrophilic surface of the nanoparticle becomes hydrophobic, allowing the adsorption of several types of drugs as well as increasing the stability of the mesoporous structure.[6] Among the functional groups which can be introduced, the amine group (–NH_2) is most commonly used to introduce a basic character to the particle. It allows the immobilization of molecules[7,8] bearing amine-reactive functional groups such as carboxylic acids with the formation of an amide bond (HN–C=O), or isocyanate groups, to give urea bonds.

The one-pot synthesis is an alternative route for grafting and is based on an *in situ* reaction of the alkoxysilane bearing the desired functional groups with the main silica precursor. Different mechanisms for the formation of mesoporous phases have been proposed, namely the liquid crystal templating (LCT) process at high surfactant concentration and the cooperative templating mechanism (CTM) at low surfactant concentrations.[9]

The same alkoxysilanes used in the grafting process can be used in the one-pot approach and are directly incorporated into the growing silica network during synthesis.[9,10] In this case, surfactant extraction in acidic media is usually applied.[11–16] In the one-pot synthesis, the possible incorporation of organic groups within the inner walls of the mesopores, due to the chemical properties and intrinsic interactions between the precursor and the micelle, can reduce the number of functional groups exposed at the surface.[17] The grafting technique does not affect the mesoporous nanoparticle structure, but it has some drawbacks such as low charge control and poor control on the distribution of the desired organic groups which are located, assuming a statistical distribution, mainly on the inner surface of the pores, which accounts for about 95% of the total surface, decreasing their size as a consequence of the steric hindrance.[18] Furthermore, some application require selectively functionalizing the inner and the outer surface of mesoporous silica nanoparticles. For this purpose, different approaches can be used, such as pre-modification of the outer surface by converting all available silanol groups with highly reactive group able to selectively react with the outer groups (usually due to steric hindrance). In a second step, the desired functional groups can be introduced to the inner wall by grafting. Another approach consist in the material functionalization before removing the surfactant.[19] In this case, the diffusion through the channels is blocked by the surfactant; however, the treatment is not always effective with small precursors since there is always the possibility of these to partially enter the channels.[20]

Among different types of ordered mesoporous silicas, MCM-41, firstly developed by researchers at the Mobil Oil Corporation in 1992,[3] is the most studied material for drug delivery systems due to its high surface area, large pores and versatility for organic functionalization. Focusing on nanomedicine, MCM-41 can be easily obtained in form of nanoparticles (MSN).[21] In general, TEOS (tetraethoxysilane) is used as Si source and CTAB (cetyltrimethylammonium bromide) is used as a modelling micellar agent.[1,3] Nanoparticles with different modifications and applications have been used in bioimaging,[19] drug delivery and photodynamic therapy,[24,25] delivery of anticancer drugs,[8,26,27] delivery of proteins by hybrid organosilica nanocapsules[28] and in many other applications.[29] The application of MSN in the biomedical area is gaining more and more attention.[23] In parallel, this has also led to studies of protein adsorption on the nano-particle surface gaining strength,[30] since this adsorption can be beneficial[31] or even impair the nanoparticles' medicinal effectiveness.[32] In particular, the formation of a protein layer on nanoparticles' surface can modify key physicochemical properties of the nanoparticles, thus affecting biodistribution, clearance, cell uptake, and other parameters. In this study, 3-aminopropyltriethoxysilane (APTES)-modified mesoporous silica nanoparticles (NH_2MSN) were prepared following two different methods, co-condensation and grafting. A low APTES loading (7%) was used in order to avoid mutual interaction between neighboring amino groups, which is detrimental for further functionalization for biomedical applications. This loading was chosen on the basis of a previous work that was considering high APTES loading (12%) on mesoporous MCM-41 to explore the limitations of the functionalization procedure.[33]

Extensive physicochemical characterization was carried out and the evaluation of spectroscopic properties of anchored photosensitizer was used to evidence any possible differences in the homogeneity of distribution of functional groups introduced by co-condensation or grafting. This is a key property to obtain an optimized nanoplatform for biomedical applications. Finally, Bovine Serum Albumin (BSA), due to its high degree of homology with human serum albumin, was chosen as a model protein to investigate the adsorption capacity of proteins on functionalized silica nanoparticles and its important role in influencing the aggregation state of nanoparticles.[34–40] Both bare and amino-modified MSN, in fact, may undergo aggregation processes in aqueous media and aggregation processes need to be bypassed or carefully evaluated for their hazard in clinical applications.

2. Results and Discussion

Amino-modified mesoporous silica nanoparticles (NH_2MSN) were prepared by following two different approaches: post-synthetic grafting of 3-aminopropyltriethoxysilane (APTES) over calcined MSN and co-condensation of APTES and TEOS in a one-pot synthesis. Calcined and amino-modified MSN were characterized by XRD, TEM and volumetric analyses to obtain information on the textural properties and on the maintenance of the mesoporous structure upon the functionalization by grafting and co-condensation methods.

X-ray diffraction patterns of NH_2MSN prepared by co-condensation (NH_2MSN(OP)) and grafting (NH_2MSN(G)) procedures are reported in Figure 1 and contrasted with the XRD pattern of calcined MSN. Calcined MSN shows the typical low-angle diffraction pattern of MCM-41 ordered systems with well-

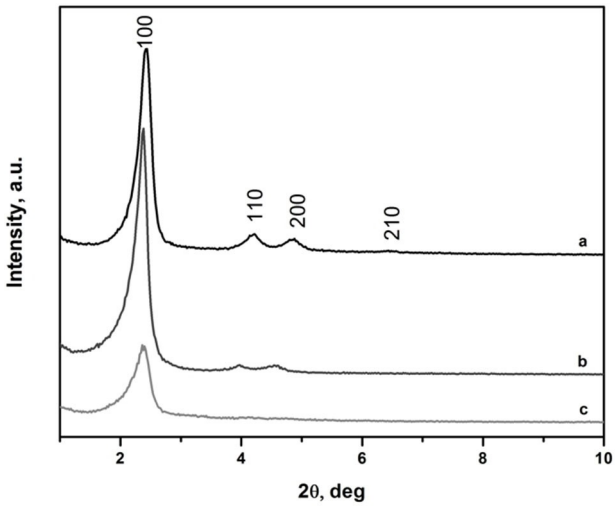

Figure 1. XRD patterns of calcined MSN (curve a), amino-modified MSN by co-condensation synthesis, NH_2MSN(OP), after SDA removal by Soxhlet extraction (curve b), and amino-modified MSN by grafting, NH_2MSN(G) (curve c).

resolved (100), (110), (200) and partially resolved (210) reflections indicating an hexagonal (p6 mm) network of mesopores with long range order.[43,44] Although both co-condensation and post-synthesis amino-modified MSN maintain the XRD pattern typical of MCM-41, the decrease in the intensity of the latter peaks could be an indication of the inclusion of the functional groups inside the pores, which lead to a decrease in the scattering contrast between pores and walls.[43–46] The different extraction methods applied for the removal of the surfactant in the case of NH_2MSN prepared by co-condensation method have different effects on the integrity of the mesoporous structure. Soxhlet extraction (curve b in Figure 1) does not affect the integrity of the mesoporous structure; in contrast, extraction in acidified methanol for 6 or 16 h severely affects the mesoporous structure (Figure S1, Supporting Information). Transmission electron microscopy (TEM) imaging (Figure 2) revealed that MSN have a regular and homogeneous shape with an average size of about 140–170 nm and with an ordered arrangement of hexagonal pores.[19,25] Neither the grafting procedure nor the co-condensation method, followed by SDA (structure-directing agent) extraction, affected the structure and morphology of MSN.

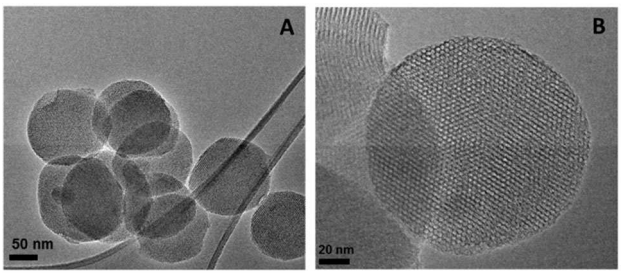

Figure 2. Representative TEM images of NH_2MSN(OP) nanoparticles.

Volumetric analysis by N_2 adsorption/desorption isotherms at 77 K were performed on calcined MSN and on the amino-modified samples. Calcined MSN presented a type IV isotherm with an H1-type hysteresis loop, typical of mesoporous materials with one-dimensional cylindrical channels (see Figure S2 in the Supporting Information). Upon functionalization with APTES, a deviation from the expected H1-type loop was observed; similar behavior in literature is usually attributed to pore size reduction upon functionalization with organosilanes.[47,48] Furthermore, we witnessed a decrease in the specific surface area (SSA), pore width and pore volume (see Table 1) which was much more severe in the case of NH_2MSN(OP), due to a residual fraction of SDA within the pores.

Thermogravimetric profiles of calcined MSN and NH_2MSN prepared by grafting or co-condensation procedure are reported in Figure 3. TGA data were normalized to the weight of dry samples (after weight loss in the range 30–180 °C due to removal of physisorbed water). In the case of calcined MSN, a limited (ca. 3 %) monotonous weight loss is evidenced, ascribable to a gradual dehydroxylation of surface silanol groups at high temperature. For the NH_2MSN(G) sample, prepared by post-synthetic grafting, three regions can be identified in the decomposition profile. The first one, from 180 to about 500 °C, can be ascribed to the condensation of silanol groups and consequent water loss, referring to silanol groups of the silica surface which were not involved in the grafting as well as to the Si atoms of mono- or bi-legged alkylsiloxane groups.[47–51] The second region is characterized by a steeper slope and goes from ca. 500 °C to about 700 °C; the weight loss in this region results from the decomposition of bound phases and can be used for the estimation of the amount of grafted functional

Table 1. Textural properties of calcined and amino-modified MSN.

Sample	SSA_{BET} [$m^2 g^{-1}$]	D_{DFT} [Å]	V [$cm^3 g^{-1}$]
MSN calcined	1250	38	1.5
NH_2MSN(OP)	150	35	0.13
NH_2MSN(G)	708	34.1	0.54

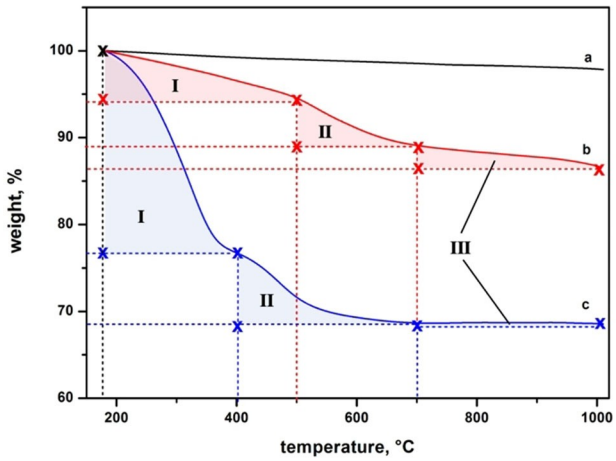

Figure 3. TGA curves of calcined MSN (curve a, black), NH_2MSN(G) (curve b, red) and NH_2MSN(OP) (curve c, blue). Ranges of integration are indicated as shadowed regions.

groups (Table 2). The third region, from about 700 °C to 1000 °C, is ascribed to further gradual dehydroxylation of the silica surface.

The decomposition profile of NH_2MSN(OP) is quite different, being dominated by a first weight loss in the 180–400 °C region which is mainly due to the residual presence of SDA within the pores of NH_2MSN(OP), as confirmed by the TGA profiles of as-prepared MSN (before calcination) and as-prepared NH_2MSN(OP) (before Soxhlet extraction) re-ported in Figure S3 in the Supporting Information. Decomposition of the amino-propyl chain is responsible of the second weight loss, in the range between 400 and 700 °C, which accounts for about 7% of the total weight loss. Weight loss at temperatures above 700 °C is negligible. Mass loss percentage corresponding to the differ-ent temperature ranges considered are reported in Table 2.

From Table 2, it can be noted that the NH_2-MSN obtained from co-condensation synthesis still contains a fraction of SDA within the pores, as the extraction procedure cannot ensure its complete removal. The weight loss related to the decomposi-tion of aminopropyl chain allowed to estimate that a 5 wt% and 7 wt% loading of APTES was achieved in NH_2MNS(G) and NH_2MSN(OP), respectively.

The successful functionalization with aminopropyl groups was further confirmed by FTIR spectroscopy (see Figure S4 in the Supporting Information). In spectra of both NH_2MNS(G) and NH_2MSN(OP), the typical signals corresponding to symmetrical and asymmetrical stretching vibrations of amino groups are observed in the high frequency range (3305 and 3365 cm^{-1}), whilst the corresponding bending mode is responsible for the signal at around 1600 cm^{-1}. The C–H stretching modes of the methylene groups of the aminopropyl chain give rise to signals in the 2800–2980 cm^{-1} range; typical absorptions ascribable to the corresponding bending modes are observed in the low frequency range (between 1450 and 1500 cm^{-1}). In the case of NH_2MSN(OP), the region of stretching and bending modes of C–H groups is perturbed by the presence of signals due to residual molecules of CTAB surfactant, as expected based on the results of TGA and volumetric analysis. Nevertheless, it has been demonstrated in previous studies that residual surfactant is removed easily during the subsequent grafting necessary to further functionalize the NH_2MSN(OP).[24]

Although the presented results showed that both techni-ques work satisfactorily for the production of amino-functional-ized mesoporous silica nanoparticles, no clear indication about the homogeneous/inhomogeneous distribution of functional groups was given.

When covalent linking of active molecules (e.g. fluoro-phores, drugs, photosensitizers, molecules for active targeting, etc.) is needed, the homogeneous distribution of anchoring groups (e.g. APTES) is of utmost importance. As an example, the electronic properties of photosensitizers, the ISC (Inter System Crossing) and the triplet excited state yields are particularly perturbed by aggregation phenomena.[52–54] In order to indirectly evidence the different distribution of NH_2 groups in NH_2MSN prepared with the two different synthetic methods, Verteporfin (Ver), a hydrophobic photosensitizer which easily form aggregates in aqueous media, was covalently bound through amide bond formation between the terminal carboxylic group of Ver and amino groups of APTES. Ver-NH_2MSN(G) and Ver-NH_2MSN(OP) were prepared with a nominal loading of 4 wt%; the appropriate loading was chosen on the basis of previous work.[55] In Figure 4A, the DR-UV-Vis spectra of the two Ver-grafted samples are shown and contrasted with the spectrum of Ver in methanol solution. As previously observed,[53] Ver immobilization on a solid support leads to a modification of

Table 2. Weight loss Δwt [%] calculated from the TGA analysis.

Sample	Range I: Δwt [%]	Range II: Δwt [%]	Range III: Δwt [%]
MSN calcined	2*	–	1[d]
NH_2MSN(G) grafting	6[a]	5[c]	3[d]
NH_2MSN(OP) post extraction	24[b]	7[c]	0.3*

[a] Weight loss due to dehydroxylation between 180 °C and 500 °C; [b] weight loss due to elimination of the CTAB surfactant between 180 °C and 400 °C; [c] weight loss due to elimination of APTES-derived groups between 400 °C and 700 °C; [d] weight loss due to further dehydroxylation between 700 °C and 1000 °C.

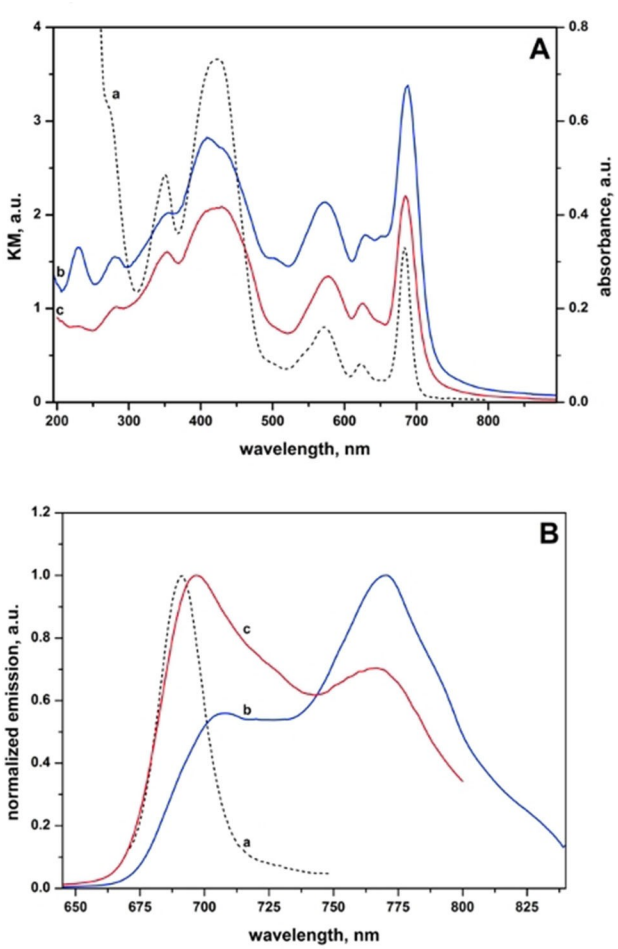

Figure 4. A) UV-Vis absorption spectrum of Ver in methanol (curve a, black dashed line) and DR-UV-Vis spectra of Ver-NH_2MSN(G) (curve b, blue solid line) and Ver-NH_2MSN(OP) (curve c, red solid line) B) Fluorescence spectra of Ver in methanol (curve a, black dashed line), Ver-NH_2MSN(G) (curve b, blue solid line) and Ver-NH_2MSN(OP) (curve c, red solid line).

the absorption spectrum; in addition to a general broadening of all bands, an increase in the relative intensity of the Q bands (in particular the component at ca. 690 nm) with respect to the Soret band is visible. The presence of Ver aggregates has been monitored by fluorescence spectroscopy. Whilst Ver in monomeric form is characterized by a fluorescence spectrum centered at ca. 695 nm, Ver aggregates display red-shifted fluorescence components (ca.775 nm). Fluorescence spectra of Ver-NH_2MSN(G) and Ver-NH_2MSN(OP), Figure 4B, suggested that aggregation phenomena are present in both cases; nevertheless, Ver-NH_2MSN(G) showed a higher intensity of the signal due to Ver aggregates compared to Ver-NH_2MSN(OP).

When Ver is grafted on solid support, the formation of molecular aggregates (e.g. dimers) depends on the degree of uniformity of NH_2 group distribution on the silica surface.

The more uniformly distributed the amino groups are on the surface, the further apart the Ver molecules will be and the less likely they are to form aggregates. In light of the fluorescence behavior, we can conclude that the functionalization of MSN with APTES through the co-condensation procedure ensures a more homogeneous distribution of the functional groups on the MSN surface. Thus, the NH_2MSN(OP) nanoparticle was selected for the study of adsorption with the BSA model protein.

When nanoparticles come into contact with biological media (e.g. serum), proteins present in such media will adsorb onto the nanoparticles' surface in an extent depending on the biological media's composition and on the surface features of the nanoparticles. The protein adsorption layer (also known as protein corona) can severely affect properties such as biodistribution, cell uptake and clearance through the modification of key physicochemical properties of the nanoparticles (e.g. the aggregation behavior). Since albumins represent one of the most abundant class of proteins in serum, adsorption studies with BSA (Bovine Serum Albumin) as a model protein were conducted with the MSN and NH_2MSN(OP) nanoparticles. BSA is widely used as a model protein to study protein corona formation for various types of nanoparticles, due to the huge amount of literature data available, the high degree of homology with human serum albumin and its low cost.[38,54,55]

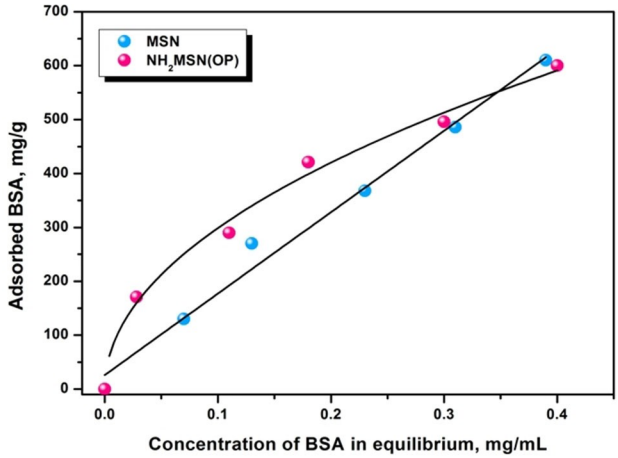

Figure 5. BSA adsorption isotherm in MSN and NH_2MSN(OP) (pH = 7.4). The black lines are drawn as a visual guidance.

The adsorption of BSA on MSN and NH_2MSN(OP) was carried out in MacIlvaine buffer (pH 7.4), according to a literature procedure,[37] and the data points for the adsorption isotherms were recorded using a 1 mg mL^{-1} BSA solution. As shown in Figure 5, the maximum adsorption capacity of BSA on the nanoparticles resulted to be about 600 mg g^{-1} for both nanoparticles. These results demonstrate that silica nanoparticles are materials with high adsorption capacity towards to BSA.

The BSA adsorption isotherms in the nanoparticles were fitted according to three classical models to describe the adsorption equilibrium within applications in the liquid phase (Table 3 and Figure S5 in the Supporting Information): Langmuir, Freundlich and Sips.

In the corresponding equations (Table 3), q_e and Q_{max} are the equilibrium and the maximum mass adsorbed per unit mass of the substrate, respectively; C_e is the equilibrium protein concentration, and K_L, K_F, K_S, 1/n and n are constants. The optimum isothermal relationship was achieved by fitting the adsorption data to the linearized forms of the Langmuir and Freundlich equations. For the Sips model, the three parameters of this equation were determined by nonlinear regression analysis.

Table 3. Parameters and correlation coefficients (R^2) of BSA adsorption equilibrium isotherms on MSN and NH_2MSN(OP) nanoparticles [pH = 7.4 and T = 37 °C].

Isotherms	Equation	Parameters		R^2	
		MSN	NH_2MSN (OP)	MSN	NH_2MSN (OP)
Langmuir	$\frac{C_e}{q_e} = \frac{1}{q_{máx} K_L} + \frac{C_e}{q_{máx}}$	K_L = 0.621 mL mg^{-1} q_m = 305 mg g^{-1}	K_L = 7.198 mL mg^{-1} q_m = 763 mg g^{-1}	0.79	0.93
Freundlich	$logq_e = \frac{1}{n} logC_e + logK_F$	K_F = 1360 mL g^{-1} 1/n = 0.857	K_F = 897 mL g^{-1} 1/n = 0.472	0.98	0.98
Sips	$\frac{1}{q_e} = \frac{1}{Q_{máx} K_S} \left(\frac{1}{C_e}\right)^{1/n} + \frac{1}{Q_{máx}}$	K_S = 10.76 mL mg^{-1} Q_{max} = 752 mg g^{-1} n = 1.48	K_S = 0,73 mL mg^{-1} Q_{max} = 472 mg g^{-1} n = 0.28	0.99	0.99

The correlations obtained from the Sips model (Figure S5A in the Supporting Information) were shown to have better adjustments than those using the Langmuir (Figure S5B) or Freundlich (Figure S5C) models. The Langmuir model is based on a reversible monolayer adsorption process involving the exchange of adsorbed proteins and free proteins in the absence of intermolecular interactions, as well as assuming a limiting amount of adsorption. In contrast, the Freundlich is an empirical model that allows molecular interactions between the surface and the adsorbate, as well as for adsorbate-adsorbate interactions in solution, forming multilayers.[57] The Sips isotherm is a combined form of the Langmuir and Freundlich models to predict heterogeneous adsorption systems, bypassing the limitation of the increasing adsorbate concentration predicted by the Freundlich isotherm. At low adsorbate concentrations, the equation is reduced to the Freundlich model, while at high concentrations, the model assumes monolayer adsorption characteristic of the Langmuir isotherm.[58,59] In Table 3 and Figure S5 in the Supporting Information, it is possible to verify that the Sips isotherm model was the best fit for the experimental data, as before mentioned. However, analyzing all data and parameters is always of great importance in order to conclude which is the most appropriate model. Since there is no limit to the adsorption capacity for Freundlich's model and the data did not reach equilibrium, this model can describe the system with relatively good linear correlation values of 0.977 and 0.982 for MSN and NH_2MSN(OP), respectively. The literature reports that for $n=1$, the isotherm presents a linear characteristic, $n>1$ presents a favorable isotherm and, finally, $n<1$ corresponds to an unfavorable isotherm.[55] The results show that NH_2MSN(OP) ($n=2.12$) is more favorable to adsorption of the model protein than MSN ($n=1.16$) according to the Freundlich model.

The Langmuir isotherm fit results show that this model does not quantitatively describe the MSN nanoparticles. It is important to emphasize that the parameter K_L, which refers to the affinity or equilibrium adsorption constant, presented a much lower value than expected. On the other hand, NH_2MSN(OP) presented a concave curve profile in the abscissa region, corresponding to a greater linear correlation possessing a favorable characteristic to the Langmuir model. Ma et al.[38] studied the interaction of BSA with silica nanoparticles modified with Cu^{2+} complexes and found good correspondence to the Langmuir model due to the specific electrostatic interactions between the histidine residues of BSA and the Cu^{2+} chelate. In this case, we can infer this small response of NH_2MSN(OP) also to the electrostatic interactions with the added amino groups. The results of the models therefore indicate that BSA adsorption to silica nanoparticles is more complicated than the ideal process described by the Langmuir model. Both protein-protein and protein-surface interactions are important in this process. In contrast to the Langmuir model, the n-constant of the Sips model is used as an indicator of surface heterogeneity.[58] This parameter decreases with increasing heterogeneity, as is the case of NH_2MSN(OP) ($n=0.28$) and, for MSN that were characterized by $n>1$, the literature proposes the formation of more than one layer of adsorbate on the adsorbent.

The mesoporous silica nanoparticles studied have heterogeneous surfaces, where parts present the pores' entrances and others correspond to their wall. Han et al. found that the adsorption of the same standard protein (BSA) with colloidal silica was best described by the Freundlich isotherm.[62] In addition, NH_2MSN(OP) are hybrid materials, where the organic parts derived from APTES can modify the way the protein interacts with these nanoparticles. Furthermore, diverse aggregation and electrostatic forces govern the process of disaggregation and interaction with other molecules/proteins.

The effect of adsorbed BSA on the colloidal stability and aggregation behavior of the nanoparticles was investigated by Dynamic Light Scattering (DLS) and zeta (ζ) potential measurements. The nanoparticles' size distribution graphs are reported in the Supporting Information (Figure S6) and the obtained data are summarized in Table 4. In the absence of BSA, both pristine calcined MSN and NH_2MSN(OP) severely aggregate when suspended in buffer at pH 7.4, with aggregates exceeding the average size of 10 μm and polydispersity indexes approaching or exceeding the value of 1. In the presence of adsorbed BSA, a considerable decrease in aggregate size was observed, with the average aggregate size decreasing along with the increase in adsorbed BSA. The dispersant effect of BSA was particularly evident in the case of NH_2MSN(OP), which reached monodispersion in the case of the highest amount of BSA tested. This observation suggests that amino-modified nanoparticles can benefit from the protein corona formation, which can avoid severe aggregation in biological media. The zeta potential of MSN and NH_2MSN(OP) was measured in absence and in presence of adsorbed BSA, and the obtained values are reported in Table S1. Pristine calcined MSN are characterized by a negative ζ potential (−17.2 mV) due to the presence of deprotonated silanol groups; on the contrary, the protonation of amino groups at pH 7.4 leads to a weakly positive ζ potential in the case of NH_2MSN(OP) (+5 mV). The ζ potential of both types of nanoparticle is modified upon adsorption of BSA. In particular, we observed an increase in the ζ potential value in

Table 4. Nanoparticle average sizes after interaction with different concentrations of BSA at pH 7.4. The initial values of MSN and NH_2MSN(OP) are in absence of BSA and the 0.2 to 1.0 BSA nomenclatures refer to interactions at different concentrations of BSA [mg mL^{-1}] after 2 h of equilibration and after removal of the unbound fraction. The measurements were performed in triplicate.

Samples	Average size[a] [nm]	Polydispersity index[a] (PDI)
MSN	6250 ± 4862	1.164 ± 0.8
MSN (0.2 BSA)	5417 ± 1032	0.643 ± 0.5
MSN (0.4 BSA)	1601 ± 548	0.427 ± 0.4
MSN (0.6 BSA)	1243 ± 426	0.353 ± 0.4
MSN (0.8 BSA)	1092 ± 405	0.319 ± 0.3
MSN (1.0 BSA)	690 ± 502	0.373 ± 0.3
NH_2MSN(OP)	5236 ± 3054	0.999 ± 0.6
NH_2MSN(OP) (0.2 BSA)	5100 ± 1584	0.567 ± 0.5
NH_2MSN(OP) (0.4 BSA)	813 ± 325	0.247 ± 0.5
NH_2MSN(OP) (0.6 BSA)	478 ± 125	0.203 ± 0.3
NH_2MSN(OP) (0.8 BSA)	432 ± 104	0.227 ± 0.2
NH_2MSN(OP) (1.0 BSA)	203 ± 58	0.264 ± 0.2

[a] Values are reported as mean value ± SD.

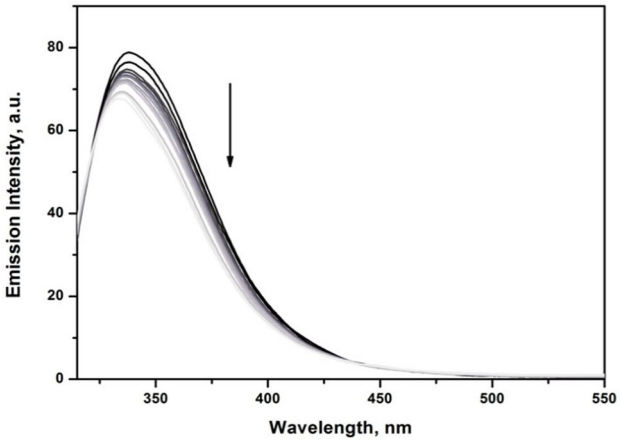

Figure 6. BSA fluorescence suppression in the presence of NH_2MSN(OP). Fluorescence spectra were obtained upon excitation at 280 nm. (Increasing NH_2MSN(OP) concentration from black to grey line, see arrow)

the case of MSN-BSA and a decrease in the case of NH_2MSN(OP), which is expected, considering that the ζ potential of BSA in solution is −10 mV. Apart from the absolute values, these ζ potential values revealed a limited colloidal stability of both MSN and NH_2MSN(OP) in the conditions tested ($+30\ mV < \zeta < -30\ mV$).

Further investigation of the dispersant effect of BSA was carried out by Resonance Light Scattering (RLS) measurements; upon addition of BSA, RLS spectra (Figure S7 in the Supporting Information) of NH_2MSN(OP) suspension underwent a decrease in intensity, which is associated with a decrease in aggregation.[62,63] The same intensity trend was observed for plain MSN (data not shown).

The interaction between nanoparticles and proteins which contain fluorescent residues, such as tryptophan and tyrosine, usually lead to fluorescence quenching. BSA has two tryptophan (Trp) residues which are responsible for the intrinsic fluorescence of BSA at about 340 nm upon excitation at 280 nm: Trp-212, located within a hydrophobic attachment pocket in the subdomain IIA, and Trp-135 on the surface of the subdomain albumin IA.[57]

Emission from these residues can be perturbed by BSA adsorption on solid surfaces, which can induce conformational changes in the protein.[64] In Figure 6, the BSA fluorescence spectra measured at increasing NH_2MSN(OP) concentrations are reported. A decrease in the fluorescence emission intensity after nanoparticle addition is observed, indicating protein-nanoparticle interaction.[65,66] Furthermore, the limited shift of the emission maximum suggests that no severe modifications of the conformation of BSA occur upon interaction.

3. Conclusion

Amino-functionalized mesoporous silica nanoparticles (MSN) were prepared by two methods, co-condensation and post-synthesis grafting of APTES. With the help of a multi-technique physicochemical characterization and further functionalization with a photosensitizer, the co-condensation method has been proved to ensure a more homogeneous distribution of amino groups on the MSN surface. The adsorption of BSA was found to be favorable, reducing the aggregation phenomena in both bare and amino-modified MSN. Nevertheless, the dispersant effect of BSA was much more evident in the case of NH_2MSN(OP), which reached monodispersion after adsorption of BSA. This suggests that amino-modified nanoparticles can benefit from protein corona formation, which can prevent severe aggregation in biological media.

Experimental Section

Materials

All reagents and solvents were purchased from Sigma Aldrich and used as received.

Methods

Synthesis of NH_2MSN by co-condensation: NH_2MSN(OP)

The co-condensation synthesis was performed according to Wada et al.[39] 0.7 g (1.9 mmol) of CTAB (cetyltrimethylammonium bromide) were dissolved in 336 mL of distilled water and to this, 2.45 mL of 2 M NaOH solution were added and the temperature was adjusted to 80 °C. TEOS (3.5 mL, 18 mmol) and APTES (0.43 mL, 2.04 mmol) were added dropwise to the medium with stirring. The mixture was stirred for 2 h and a white precipitate was obtained which was filtered and then washed with a mixture of water and ethanol. The obtained silica was dried in air for 24 h at 60 °C. For removal of the structure directing agent (SDA) through the use of solvent, two different methodologies were used:

1) The nanoparticles were introduced into a 250 mL flask with a solution of methanol plus 4 drops of 37.4% HCl and stirred for 6 and 16 h;
2) Soxhlet extraction with an isopropanol solution and 2 drops of 37.4% HCl at 200 °C for 2 days.[40]

Synthesis of NH_2MSN by grafting with APTES: NH_2MSN(G)

NH_2MSN(G) were prepared according to Parida et al.[41] by suspending 1 g of MSN nanoparticles (prepared and calcined as reported in the Supporting Information) in 30 mL toluene. APTES (0.6 g, 2.7 mmol) was added dropwise to the medium with stirring. The reaction was refluxed for 8 h and the nanoparticles were recovered by centrifugation, washed with ethanol and deionized water and dried in air at 80 °C.

Covalent anchoring of Verteporfin to NH_2MSNs

Verteporfin (Ver, 1 equiv.), 1-[bis(dimethylamino)methylene)-1H-1,2,3-triazolo[4,5-b]pyridinium-3-oxide hexafluorophosphate (HATU, 1 equiv.) and *N*,*N*-diisopropylethylamine (DIPEA, 1 equiv.) were dissolved in *N*,*N*-dimethylformamide (DMF, 10 mL) and the obtained solution was added to a suspension of NH_2MSN(OP) or NH_2MSN(G) in DMF (10 mL, 10 mg mL^{-1}). The resulting mixture was stirred vigorously at room temperature for 24 h in the dark, then the solid was recovered by filtration, washed with fresh DMF and dried under vacuum. Ver-NH_2MSN(G) and Ver-NH_2MSN(OP) were

prepared with a nominal Ver loading of 4 wt%; the appropriate loading was chosen on the basis of previous work.[54] The actual Ver loading was calculated from the UV-Vis spectra of the Ver eluate after the washing procedure, using the Lambert-Beer law ($\varepsilon = 35000\ M^{-1}\,cm^{-1}$ in DMF). The actual loadings were found to be 3.0% and 3.5% for Ver-NH_2MSN(OP) and Ver-NH_2MSN(G), respectively.

Characterization

The X-ray diffraction (XRD) analyses were performed on a ARLXTRA-18 powder diffractometer with Cu–Kα radiation ($\lambda = 1.54062$ Å), with a scanning speed of $0.01^\circ\ min^{-1}$.

The TEM images were obtained with a high-resolution transmission electron microscope JEOL 3010 at 300 kV. The samples were prepared by dispersing and sonicating in isopropanol and depositing a few drops of the suspension on copper grids coated with a carbon film.

Thermogravimetric analysis (TGA-DTGA) was performed under an argon flow (100 mL min^{-1}) with a SETSYS evolution of the TGA-DTG/DSC thermobalance, heating between 30 °C and 1000 °C at a scanning speed of 5 °C per minute.

The adsorption/desorption isotherms of N_2 were performed at 77 K at a relative pressure variation between 1×10^{-6} to 1 P/P_0 using a Quantachrome Autosorb 1 MP/TCD instrument. Prior to the start of the analysis, the samples were degassed at 373 K for 3 h. The specific surface areas were calculated using the Brunauer-Emmett-Teller (BET) equation in the relative pressure range varying from 0.01 to 0.1 P/P_0. The pore size distribution was calculated from the DFT method, using the desorption region of the N_2 physisorption isotherm.

FTIR spectra were measured on self-supported pellets in vacuum using a Bruker Equinox 55 spectrometer equipped with a DTGS piezoelectric detector working at 4 cm^{-1} resolution and 32 scans.

The dynamic light scattering (DLS) was performed at 37 °C with nanoparticles dispersed in McIlvaine buffer pH 7.4 using the Malvern Zetasizer Nano-ZS equipment, which uses a 4 mW He-Ne laser operating at 633 nm at a detection angle of 173°.

UV-Vis absorption spectra of Ver eluate and Diffuse Reflectance UV-Vis (DR UV-Vis) spectra of Ver-grafted MSNs were recorded using a Perkin Elmer Lambda 900 spectrometer equipped with a diffuse reflectance sphere attachment.

Photoemission and excitation steady state spectra were acquired with a Horiba Scientific Fluorolog spectrofluorimeter equipped with a 450 W Xenon lamp and a Hamamatsu R928 photomultiplier. The spectral response was corrected for the spectral sensitivity of the photomultiplier.

Adsorption Study with BSA Protein Model

The adsorption assays of BSA on nanoparticles (MSN and NH_2MSN(OP)) in McIlvaine buffer pH 7.4 were performed according to the literature.[37] Approximately 1 mg of the silica nanoparticles was mixed with 4 mL of various concentrations of BSA (0.2–1.0 mg mL^{-1} BSA, which is labelled with sample names) in McIlvaine [Na_2HPO_4] = [Citric acid] = 7.5×10^{-3} mol L^{-1} (pH = 7.4) with ionic strength control by [NaCl] = 0.1 mol L^{-1}. The mixtures were stirred at room temperature for 2 h. The particles were then centrifuged, and the supernatant analyzed by UV-Vis spectroscopy at 280 nm to quantify the unbound fraction of BSA. The adsorbed amount of protein was calculated by mass balance. The experiments were conducted with a Cary-50UV-Vis spectrophotometer. Fluorescence quenching and resonant light scattering experiments were performed using a Cary-Eclipse spectrofluorimeter equipped with temperature control and xenon flash lamp. For experiments involving fluorescence quenching, in a cuvette containing 5 mmol of BSA, silica nanoparticles prepared in McIlvaine buffer solution were titrated and the fluorescence was monitored by excitation at 280 nm and the reading performed at 300–550 nm. The RLS experiments were performed operating the Cary-Eclipse in synchronous mode ($\lambda_{exc} = \lambda_{emis}$), performing a 200–800 nm scan after each MSN titration in the BSA solution contained in the cuvette.[42] This principle consists of the mesoporous silica nanoparticle characterization in a self-aggregating state.

Acknowledgements

I. M. thanks Università del Piemonte Orientale for financial support (Fondi di Ateneo per la Ricerca anno 2017 – FAR 2017).

Conflict of Interest

The authors declare no conflict of interest.

Data Availability Statement

The data that support the findings of this study are available from the corresponding author upon reasonable request.

Keywords: aggregation · amino-functionalized mesoporous silica nanoparticles · BSA · co-condensation · grafting

[1] J. S. Beck, J. C. Vartuli, W. J. Roth, M. E. Leonowicz, C. T. Kresge, K. D. Schmitt, C. T. W. Chu, D. H. Olson, E. W. Sheppard, S. B. McCullen, J. B. Higgins, J. L. Schlenker, *J. Am. Chem. Soc.* **1992**, *114*, 10834–10843.
[2] C. T. Kresge, W. J. Roth, *Chem. Soc. Rev.* **2013**, *42*, 3663–3670.
[3] C. T. Kresge, M. E. Leonowicz, W. J. Roth, J. C. Vartuli, J. S. Beck, *Nature* **1992**, *359*, 710–713.
[4] P. Xu, X. Li, H. Yu, T. Xu, *Sensors* **2014**, *14*, 19023–19056.
[5] X. S. Zhao, G. Q. Lu, A. K. Whittaker, G. J. Millar, H. Y. Zhu, *J. Phys. Chem. B* **1997**, *101*, 6525–6531.
[6] J. C. Doadrio, E. M. B. Sousa, I. Izquierdo-Barba, A. L. Doadrio, J. Perez-Pariente, M. Vallet-Regí, *J. Mater. Chem.* **2006**, *15*, 462–466.
[7] T. Shigeno, M. Nagao, T. Kimura, K. Kuroda, *Langmuir* **2002**, *18*, 8102–8107.
[8] B. Martins Estevão, E. Comparetti, N. Rissi, V. Zucolotto, *Mater. Adv.* **2021**, *2*, 5224–5235.
[9] J. L. Blin, M. Impéror-Clerc, *Chem. Soc. Rev.* **2013**, *42*, 4071–4082.
[10] J. Kobler, K. Möller, T. Bein, *ACS Nano* **2008**, *2*, 791–799.
[11] K. Möller, J. Kobler, T. Bein, *J. Mater. Chem.* **2007**, *17*, 624–631.
[12] K. F. Lam, K. Y. Ho, K. L. Yeung, G. McKay, *Stud. Surf. Sci. Catal.* **2004**, *154 C*, 2981–2986.
[13] E. Gianotti, U. Diaz, A. Velty, A. Corma, *Catal. Sci. Technol.* **2013**, *3*, 2677–2688.
[14] C. Ivaldi, I. Miletto, G. Paul, G. B. Giovenzana, A. Fraccarollo, M. Cossi, L. Marchese, E. Gianotti, *Molecules* **2019**, *24*, 848.
[15] M. H. Lim, A. Stein, *Chem. Mater.* **1999**, *11*, 3285–3295.
[16] D. Brühwiler, *Nanoscale* **2010**, *2*, 887–892.
[17] R. J. Soto, L. Yang, M. H. Schoenfisch, *ACS Appl. Mater. Interfaces* **2016**, *8*, 2220–2231.
[18] E. Ruiz-Hitzky, S. Letaïef, V. Prévot, *Adv. Mater.* **2002**, 439–443.
[19] A. Molnar, B. Rac, *Curr. Org. Chem.* **2006**, *10*, 1697–1726.

[20] B. Martins Estevão, I. Miletto, L. Marchese, E. Gianotti, *Phys. Chem. Chem. Phys.* **2016**, *18*, 9042–9052.
[21] D. S. Shephard, W. Zhou, T. Maschmeyer, J. M. Matters, C. L. Roper, S. Parsons, B. F. G. Johnson, M. J. Duer, *Angew. Chem. Int. Ed.* **1998**, *37*, 2719–2723; *Angew. Chem.* **1998**, *110*, 2847–2851.
[22] Z. Shariatinia, Z. Zahraee, *J. Colloid Interface Sci.* **2017**, *501*, 60–76.
[23] J. Lu, M. Liong, J. I. Zink, F. Tamanoi, *Small* **2007**, *3*, 1341–1346.
[24] M. Vallet-Regí, M. Colilla, I. Izquierdo-Barba, M. Manzano, *Molecules* **2018**, *23*, 47.
[25] E. Gianotti, B. Martins Estevão, F. Cucinotta, N. Hioka, M. Rizzi, F. Renò, L. Marchese, *Chem. A Eur. J.* **2014**, *20*, 10921–10925.
[26] M. Rizzi, S. Tonello, B. M. Estevão, E. Gianotti, L. Marchese, F. Renò, *J. Photochem. Photobiol. B* **2017**, *167*, 1–6.
[27] A. Bertucci, E. A. Prasetyanto, D. Septiadi, A. Manicardi, E. Brognara, R. Gambari, R. Corradini, L. De Cola, *Small* **2015**, *11*, 5687–5695.
[28] V. Giglio, S. Varela-Aramburu, L. Travaglini, F. Fiorini, P. H. Seeberger, L. Maggini, L. De Cola, *Chem. Eng. J.* **2018**, *340*, 148–154.
[29] E. A. Prasetyanto, A. Bertucci, D. Septiadi, R. Corradini, P. Castro-Hartmann, L. De Cola, *Angew. Chem. Int. Ed.* **2016**, *55*, 3323–3327; *Angew. Chem.* **2016**, *128*, 3384–3388.
[30] B. Yang, Y. Chen, J. Shi, *Adv. Healthcare Mater.* **2018**, *7*, 1800268.
[31] W. Xiao, H. Gao, *Int. J. Pharm.* **2018**, *552*, 328–339.
[32] R. Cagliani, F. Gatto, G. Bardi, *Materials* **2019**, *12*, 1–11.
[33] C. D. Walkey, J. B. Olsen, H. Guo, A. Emili, W. C. W. Chan, *J. Am. Chem. Soc.* **2012**, *134*, 2139–2147.
[34] P. Iliade, I. Miletto, S. Coluccia, G. Berlier, *Res. Chem. Intermed.* **2012**, *38*, 785–794.
[35] J. Saikia, M. Yazdimamaghani, S. P. Hadipour Moghaddam, H. Ghandehari, *ACS Appl. Mater. Interfaces* **2016**, *8*, 34820–34832.
[36] Z. Yang, H. Ma, Z. Jin, H. Cao, L. Lei, Y. Ma, Z. Lei, *New J. Chem.* **2017**, *41*, 1637–1644.
[37] S. Dominguez-Medina, S. McDonough, P. Swanglap, C. F. Landes, S. Link, *Langmuir* **2012**, *28*, 9131–9139.
[38] Z. Ma, Y. Guan, H. Liu, *J. Magn. Magn. Mater.* **2006**, *301*, 469–477.
[39] V. Nairi, S. Medda, M. Piludu, M. F. Casula, M. Vallet-Regì, M. Monduzzi, A. Salis, *Chem. Eng. J.* **2018**, *340*, 42–50.
[40] A. Wada, S. Tamaru, M. Ikeda, I. Hamachi, *J. Am. Chem. Soc.* **2009**, *131*, 14, 5321–5330.
[41] F. Carniato, M. Muñoz-Úbeda, L. Tei, M. Botta, *Dalton Trans.* **2015**, *44*, 17927–17931.
[42] K. M. Parida, D. Rath, *J. Mol. Catal. A* **2009**, *310*, 93–100.
[43] R. F. Pasternack, P. J. Collings, *Science* **1995**, *269*, 935–939.
[44] B. Martins Estevão, F. Cucinotta, N. Hioka, M. Cossi, M. Argeri, G. Paul, L. Marchese, E. Gianotti, *Phys. Chem. Chem. Phys.* **2015**, *17*, 26804–26812.
[45] K. P. S. Zanoni, R. R. C. Vilela, I. D. A. Silva, N. Y. Murakami Iha, H. Eckert, A. S. S. De Camargo, *Inorg. Chem.* **2019**, *58*, 4962–4971.
[46] M. Abdouss, N. Hazrati, A. A. Miran Beigi, A. Vahid, A. Mohammadalizadeh, *RSC Adv.* **2014**, *4*, 6337–6345.
[47] A. C. P. da Silva, P. H. Y. Cordeiro, B. M. Estevão, W. Caetano, H. Eckert, S. M. O. Santin, M. P. Moisés, N. Hioka, A. L. Tessaro, *J. Braz. Chem. Soc.* **2019**, *30*, 1599–1607.
[48] C. Schlumberger, M. Thommes, *Adv. Mater. Interfaces* **2021**, *8*, 2002181.
[49] P. Gao, C. Yang, Z. Liang, W. Wang, Z. Zhao, B. Hu, F. Cui, *Chemosphere* **2019**, *214*: 361–370.
[50] M. Jaroniec, C. P. Jaroniec, M. Kruk, R. Ryoo, *Adsorption* **1999**, *5*, 313–317.
[51] K. C. Vrancken, P. Van Der Voort, I. Gillis-D'Hamers, E. F. Vansant, P. Grobet, *J. Chem. Soc. Faraday Trans.* **1992**, *88*, 3197–3200.
[52] G. E. Musso, E. Bottinelli, L. Celi, G. Magnacca, G. Berlier, *Phys. Chem. Chem. Phys.* **2015**, *17*, 13882–13894.
[53] A. B. Ormond, H. S. Freeman, *Materials* **2013**, *6*, 817–840.
[54] T. Kobayashi, J-Aggregates Vol.2, World Scientific Publishing Co. Pte. Ltd. Singapore, **2012** p.49.
[55] E. Gianotti, B. M. Estevão, I. Miletto, S. Tonello, F. Renò, L. Marchese, *ChemistrySelect* **2016**, *1*, 127–131.
[56] C. Y. Lin, C. M. Yang, M. Lindén, *RSC Adv.* **2019**, *9*, 33912–33921.
[57] F. Catalano, G. Alberto, P. Ivanchenko, G. Dovbeshko, G. Martra, *J. Phys. Chem. C* **2015**, *119*, 26493–26505.
[58] W. Li, S. Li, *Colloids Surf. A* **2007**, *295*, 159–164.
[59] K. Y. Foo, B. H. Hameed, *Chem. Eng. J.* **2010**, *156*, 2–10.
[60] R. Sips, *J. Chem. Phys.* **1948**, *16*, 490–495.
[61] G. Liu, J. Ma, X. Li, Q. Qin, *J. Hazard. Mater.* **2009**, *164*, 1275–1280.
[62] J. Han, P. Silcock, A. J. McQuillan, P. Bremer, *Colloids Surf. A* **2009**, *349*, 207–213.
[63] M. Ren, S. Wang, C. Cai, C. Chen, X. Chen, *RSC Adv.* **2016**, *6*, 83078–83083.
[64] W. Lu, B. S. Fernández Band, Y. Yu, L. Q. Geng, J. C. Shang, C. Wang, Y. Fang, R. Tian, L. P. Zhou, L. L. Sun, Y. Tang, S. H. Jing, W. Huang, J. P. Zhang, *Microchim. Acta* **2007**, *158*, 29–58.
[65] S. Ranjan, N. Dasgupta, P. Srivastava, C. Ramalingam, *J. Photochem. Photobiol. B* **2016**, *161*, 472–481.
[66] K. Bolaños, F. Celis, C. Garrido, M. Campos, F. Guzmán, M. J. Kogan, E. Araya, *J. Mater. Chem. B* **2020**, *8*, 8644–8657.

Manuscript received: October 1, 2021
Revised manuscript received: November 30, 2021